Nanomedicine: Nanotechnology, Biology, and Medicine
xx (xxxx) xxx

nanomedicine
Nanotechnology, Biology, and Medicine

nanomedjournal.com

Design of a mediator-free, non-enzymatic electrochemical biosensor for glutamate detection

Elnaz Zeynaloo, MS[a,b], Yu-Ping Yang, PhD[a,c], Emre Dikici, PhD[a,c], Ralf Landgraf, PhD[a], Leonidas Bachas, PhD[b,c,*], Sylvia Daunert, PhD[a,c,d,**]

[a]*Department of Biochemistry and Molecular Biology, , Miller School of Medicine, University of Miami, Miami, Florida, United States*
[b]*Department of Chemistry, University of Miami, Miami, Florida, United States*
[c]*Dr. JT Macdonald Foundation Biomedical Nanotechnology Institute, University of Miami, Miami, Florida, United States*
[d]*University of Miami Clinical and Translational Science Institute, University of Miami, Miami, Florida, United States*

Received 4 May 2020; revised 21 August 2020; accepted 14 September 2020

Abstract

A mediator-free, non-enzymatic electrochemical biosensor was constructed by covalent immobilization of a genetically engineered periplasmic glutamate binding protein onto gold nanoparticle-modified, screen-printed carbon electrodes (GluBP/AuNP/SPCE) for the purpose of direct measurement of glutamate levels. Glutamate serves as the predominant excitatory neurotransmitter in the central nervous system. As high levels of glutamate are an indicator of many neurologic disorders, there is a need for advancements in glutamate detection technologies. The biosensor was evaluated for glutamate detection by cyclic voltammetry. Binding of glutamate to the immobilized glutamate binding protein results in a conformational change of the latter that alters the microenvironment on the surface of the sensor, which is manifested as a change in signal. Dose–response plots correlating the electrochemical signal to glutamate concentration revealed a detection limit of 0.15 μM with a linear range of 0.1-0.8 μM. Selectivity studies confirmed a strong preferential response of the biosensor for glutamate against common interfering compounds.

Key words: Glutamate biosensor; Non-enzymatic; Gold nanoparticle; Screen-printed carbon electrode; Periplasmic binding protein

Glutamate serves as the major excitatory neurotransmitter in the vertebrate central nervous system. In addition to influencing sensory perception, mood, and motor control, an excess of glutamate in extracellular fluid (ECF) can cause excitotoxicity.[1] Prolonged elevated extracellular levels of glutamate eventually result in neuronal cell death, which is a common pathological process in many neurological disorders such as stroke,[2] Alzheimer's disease,[3] brain trauma,[4] and multiple sclerosis.[5] Apart from neurodegenerative diseases, glutamate is also involved in tumorigenesis, and it has been reported that some

Abbreviations: GluBP, genetically engineered periplasmic glutamate binding protein; AuNP, gold nanoparticle; SPCE, screen-printed carbon electrode; GlOx, glutamate oxidase; NiNAE, nickel nanowire array; Pt/NiNAE, platinum-coated nickel nanowire array; GCE, glassy carbon electrode; NiOGC, nickel oxide glassy carbon; Co_3O_4NS, cobalt oxide mesoporous nanosheet; CV, cyclic voltammetry; CA, chronoamperometry; EIS, electrochemical impedance spectroscopy; EDX, energy-dispersive X-ray; SEM, scanning electron microscopy; SPR, surface plasmon resonance; EDC, 1-ethyl-3-(3-dimethylaminopropyl)carbodiimide; NHS, N-hydroxysuccinimide; SDS-PAGE, sodium dodecyl sulfate polyacrylamide gel electrophoresis; PB, phosphate buffer; PBS, phosphate buffer saline; IPTG, isopropyl β-D-1-thiogalactopyrano

Acknowledgments
The authors declare that they have no conflict of interest.
This work was presented in the following meetings:

1-NanoFlorida 2019 International Conference, Tampa, Florida
2-Brain & Brain PET 2019 International Conference, Yokohama, Japan
3-Neural Engineering Symposium 2019, Miami, Florida

*Correspondence to: L. G. Bachas, Department of Chemistry, University of Miami, Miami, Florida 33134, United States.
**Correspondence to: S. Daunert, Department of Biochemistry and Molecular Biology, Miller School of Medicine, University of Miami, Miami, Florida 33136, United States.
E-mail addresses: Bachas@miami.edu, (L. Bachas), sdaunert@med.miami.edu. (S. Daunert).

https://doi.org/10.1016/j.nano.2020.102305
1549-9634/

t1.1 Table 1
t1.2 Comparison of analytical performance of non-enzymatic glutamate sensors.

t1.3 Working electrode material	Detection limit	Linear detection range	Electrolyte	Potential interferences	Ref
t1.4 NiNAE	68 μM	0.5-8 mM	1 M NaOH	Uric acid, ascorbic acid, glucose	32
t1.5 Pt/NiNAE	83 μM	0.5-8 mM	1 M NaOH	Uric acid, ascorbic acid, and glucose	32
t1.6 NiO/GCE	272 μM	1-8 mM	0.1 M NaOH	Uric acid, ascorbic acid, glucose	33
t1.7 Co_3O_4NS/GCE	10 pM	0.1 nM-0.1 M	100 mM PBS pH 7.0	Uric acid, bilirubin, aspartic acid, thiourea, glucose, glycine, cysteine, glutathione, and tyrosine	34
t1.8 GluBP/AuNP/SPCE	0.15 μM	0.1-0.8 μM	50 mM PB pH 7.4	Aspartate and ascorbic acid	current work

tumor cells enable secretion of glutamate to promote tumor growth and invasion.[6,7] Notably, in many diseases high blood levels of glutamate have been observed in diseased individuals compared to healthy ones, which suggest that glutamate could be used as a diagnostic biomarker for detection and monitoring of disease progression.[8–10]

A number of techniques have been developed for glutamate detection, such as high performance liquid chromatography,[11] capillary electrophoresis,[12] microdialysis[13] and enzyme-linked immunosorbent assay.[14] Several of them have limitations such as being time-consuming and requiring expensive instruments and highly skilled personnel to perform the tests. On the other hand, electrochemical techniques have received considerable attention because they are fast, easy to miniaturize, cost effective, and require small sample volumes, which make them well-suited for use in clinical applications, such as point-of-care testing and implantable devices.[15]

During the last decade, advances in nanotechnology and fabrication techniques have resulted in a paradigm shift in electrochemical sensing systems by coupling miniaturization with high performance and sustainability. Among the nanomaterials incorporated in electrochemical techniques, gold nanoparticles (AuNPs) have been used widely because of their excellent biocompatibility and ability to be conjugated with biomolecules with relative ease.[16–19] Moreover, incorporation of AuNPs in the body of the sensor facilitates electron transfer, improves conductivity, and provides a large electrochemically active surface area,[20] which results in increased sensitivity of the sensor.[20–23]

Biosensors based on molecular recognition principles are devices that transduce the event of ligand binding by a generating signal that is proportional to the concentration of the ligand in the sample.[24] Enzyme-based electrochemical biosensors are commonly used in the detection of analytes including glutamate. Glutamate oxidase (GlOx) has been used in preparation of glutamate biosensors and their design and fabrication have been discussed in several reviews in detail.[25–28] In principle, GlOx is incorporated onto the electrode along with a co-factor to catalyze the conversion of glutamate to α-ketoglutarate. This reaction is accompanied by the consumption of molecular oxygen and production of hydrogen peroxide (H_2O_2). The produced H_2O_2 can be detected electrochemically either through direct reduction or by employing redox mediators. Nevertheless, enzymatic electrochemical biosensors typically require redox mediators[29] and suffer from limitations, such as oxygen dependency and strong matrix interference from substances, e.g., ascorbic acid.[30]

There have been also literature reports of non-enzymatic glutamate sensors (Table 1), with Ni-based sensors receiving significant attention.[31,32] For example, Jamal et al demonstrated the application of a vertically aligned nickel nanowire array (NiNAE) and a Pt-coated nickel nanowire array (Pt/NiNAE) to detect glutamate in a highly alkaline electrolyte. This group also reported the fabrication of a nickel oxide glassy carbon electrode (NiOGCE) for the detection of glutamate.[33] Nickel oxide and nickel nanowires possess electrocatalytic activity that enables oxidation of glutamate without using glutamate oxidase. Even though the ability of the Ni-based sensor to detect glutamate is comparable to enzymatic electrochemical biosensors, this type of sensor has low selectivity toward glutamate[31] and requires a high pH environment, which is not desirable when detecting the analyte in biological samples. Hussain et al reported the fabrication of a cobalt oxide mesoporous nanosheet on glassy carbon electrode (Co_3O_4NS/GCE) to develop a non-enzymatic glutamate sensor.[34] The system works by oxidizing glutamate in the sample but suffers from several interferences that could also become oxidized.

Herein we describe a novel, mediator-free, non-enzymatic electrochemical sensor for direct glutamate detection by leveraging the genetically engineered bacterial periplasmic glutamate binding protein (GluBP) from *E. coli* and gold nanoparticle (AuNP)-modified screen-printed carbon electrodes (SPCEs). GluBP comprises two globular domains joined by a hinge forming a groove structure that exhibits a large hinge-twist conformational change upon glutamate binding.[35] When immobilized on AuNP/SPCEs, the glutamate-induced conformational change alters the microenvironment on the electrode surface which, in turn, results in a current change in response to the applied potential. In this work, for the first time, we have exploited the selective binding of GluBP to glutamate and its conformational change using an electrochemical approach. Specifically, we genetically introduced cysteine residues at the C-terminus of GluBP that can be used to covalently attach the protein to gold nanoparticles on the SPCEs through thiol-gold bonds. Further, we employed cyclic voltammetry (CV) to measure current changes upon glutamate binding. The detection limit of the biosensor was 0.15 μM. Additionally, the sensor exhibited high selectivity toward glutamate over common interfering substances and other amino acids. Overall, the sensor is active and demonstrated the highest peak current intensity at

neutral pH, which is compatible with the pH of biological samples. By excluding the use of enzymes and redox mediators, the direct measurement of glutamate is facilitated at ambient environment, where the stability of the biosensor is at its optimum.

Methods

Reagent and materials

All amino acids, ascorbic acid, gold(III) chloride trihydrate, potassium ferrocyanide, potassium ferricyanide, sodium phosphate dibasic, sodium phosphate monobasic, potassium phosphate dibasic, potassium phosphate monobasic, sodium chloride, potassium chloride, glycerol, N-hydroxysuccinimide (NHS), and ampicillin sodium salt were purchased from Sigma Aldrich (St. Louis, MO). Bromophenol blue and 0.2 μm syringe filters were purchased from VWR (Bridgeport, NJ). Imidazole was obtained from J.T. Baker (Phillipsburg, NJ). Sodium dodecyl sulfate was ordered from Curtin Matheson (Houston, TX). Luria–Bertani (LB) broth was from Becton, Dickinson and Company (Sparks, MD). Agar and 1-ethyl-3-(3-dimethylaminopropyl)carbodiimide (EDC) were purchased from Fisher Scientific (Fair Lawn, NJ). The plasmid, pDisplay FLIPE-600n, consisting of the coding region of ybeJ (GluBP) was obtained from Addgene (Watertown, MA). The pCold I expression vector was from Takara Bio (Mountain View, CA). The NEB Express Competent *E. coli* (High Efficiency) was purchased from New England Biolabs (Ipswich, MA). The Bradford protein assay kit was obtained from Bio-Rad (Hercules, CA). QIAquick gel purification kit and QIAprep DNA isolation kit were purchased from Qiagen (Valencia, CA). The BCA protein assay kit and 3500 MWCO Slide-A-Lyzer 3 mL dialysis cassettes were from Pierce (Rockford, IL). ProBlock gold extra strength [100×] (protease inhibitor), Ni-NTA agarose resin, and isopropyl β-D-1-thio-galactopyranoside (IPTG) were obtained from Gold Biotechnology (St. Louis, MO). The Mark12 protein standard and 1 kb DNA standard were purchased from Invitrogen (Carlsbad, CA). Screen-printed carbon electrodes ItalSens IS-C were purchased from PalmSens (Houten, Netherlands). Sensor Chip CM5 was obtained from GE Healthcare Life Sciences (Pittsburgh, PA). All reagents were of analytical grade and used without further purification.

Equipment

Polymerase chain reactions (PCRs) were performed using an Eppendorf Mastercycler Personal Thermocycler (Hauppauge, NY). Electrophoresis of DNA was carried out using an FB105 Fisher Biotech Electrophoresis Power Supply (Pittsburgh, PA). DNA gels were visualized using a UV Transilluminator platform from UVP (Upland, CA). The sonicator for lysing the cells was a 550 Sonic Dismembrator from Fisher Scientific. The incubator for the protein expression was a Forma Scientific Orbital Shaker (Fairlawn, NJ). All centrifugations were performed using a Beckman J2MI centrifuge (Palo Alto, CA). Proteins were visualized by sodium dodecyl sulfate polyacrylamide gel electrophoresis (SDS-PAGE) using PROTEAN TGX stain-free precast gels 4%-20% from Bio-Rad in an Invitrogen X Cell Sure Lock Mini Cell (Carlsbad, CA). Scanning electron microscopy (SEM) was used to study the morphology of the AuNPs using a Philips XL30 field-emission environmental SEM, operated at an acceleration voltage of 5 kV and a working distance of 10.1 mm for the AuNP modified SPCE and 14.9 mm for the bare SPCE. The SEM instrument was equipped with an Oxford energy-dispersive X-ray detector energy-dispersive X-Ray spectroscopy microscope (EDX). Amperometric and voltammetric measurements were performed with a PalmSens 4 electrochemical analyzer controlled by PSTrace5.3 software. Surface plasmon resonance (SPR) measurements were carried out on a Biacore T200 (GE), and data were analyzed using Biacore T200 Evaluation Software (version 1.0).

Protein expression and purification

The plasmid consisting of the coding region of ybeJ (GluBP) was obtained, and the ybeJ gene modified with a coding sequence for two cysteine residues was amplified by using PCR (forward primer: GTAGGCATATGGGA GGCGGCGCAGGCAGCACGCTGGAC and reverse primer: CTATCTAGATTAACAGCACGCGCCACCGCTAT AGTTCAGTGC-CTTGTCATTCGGTTC). The PCR product was subsequently inserted into the pCold I expression vector to give pCold I-ybeJ and transformed into competent *E. coli* NEB Express cells. The cells were grown overnight at 37 °C in 5.0 mL LB broth containing 100 μg/mL ampicillin. The pelleted cells were then grown for 4 h at 30 °C while shaking at 250 rpm in 300 mL LB broth containing 100 μg/mL ampicillin. After the optical density of the culture reached an OD_{600} of 0.9, the cells were cold-shocked for an hour at 4 °C followed by inducing them with a final concentration of 1 mM IPTG. The flask was incubated at 4 °C overnight, and the media was centrifuged at 8000 ×*g* for 20 min at 4 °C. The pellet was then resuspended in the lysis buffer containing 50 mM Na_2HPO_4, 300 mM NaCl, 10 mM imidazole, pH 8, and kept at −20 °C until use.

The frozen pellet was thawed and, after the addition of protease inhibitor, sonicated for 10 min (using 1-s on, 1-s off pulse sequence for a total of 20 min) and centrifuged at 17,000 ×*g* for 20 min at 4 °C to collect any cell debris. The supernatant was filtered through a 0.2-μm syringe filter and then purified by immobilized metal affinity chromatography using a Ni-NTA resin. The GluBP was eluted with a gradient from 10 mM to 180 mM imidazole-containing lysis buffer. The protein was then dialyzed into 50 mM phosphate buffer saline (PBS), pH 7.4. SDS-PAGE was used to determine the purity of the protein, which manifested as a single band in the gel (Figure S1). The concentration of the protein was measured by the BCA assay according to the manufacturer's instructions. The protein was diluted right before use with 50 mM phosphate buffer, pH 7.4, to reach the final concentration of 5 μM.

Fabrication and characterization of GluBP/AuNP/SPCE

The commercially available SPCEs were pretreated by sweeping the potential from −1.0 to +1.0 V at a scan rate of 300 mV/s using cyclic voltammetry in 0.5 M sulfuric acid. To generate AuNP/SPCEs, 20 μL of different concentrations

(100 μM, 1 mM, or 10 mM) of gold(III) chloride ($HAuCl_4$) in 0.5 M H_2SO_4 was used to deposit AuNP to the surface of the pretreated SPCEs.[36,37] The AuNP electrodeposition was conducted through chronoamperometry (CA) for 5 min (Figure S2) to reduce Au^{+3} to Au^0 on the surface of the working electrode.[38,39] Cyclic voltammograms of the fabricated electrodes were collected (Figure S3). The morphology and composition of the nanoparticles were examined using SEM and EDX, respectively. The size of 100 AuNPs was measured as the longest line of each particle on the micrographs, and the mean and standard deviation are reported. The cyclic voltammograms of the AuNP/SPCEs were collected by sweeping the potential from −0.2 to +1.0 V at a scan rate of 50 mV/s in 50 mM sodium phosphate buffer (PB); buffers were prepared in the pH range 3.2-8.3 (Figure S4). The presence of a significant reduction peak in the generated cyclic voltammograms indicated the successful AuNP deposition on SPCEs. The AuNP/SPCE response is pH-dependent, and by decreasing the pH, the gold reduction peak shifts to higher potential (right). The highest peak current was observed at pH 7.4 at a potential of +0.13 V vs Ag/AgCl. This pH was chosen for the remainder of the studies, because it is also compatible with the pH of biological samples. The surface of the electrodes was rinsed with PB, and then 10 μL of 5 μM GluBP was drop-cast on the surface of the AuNP/SPCE to generate GluBP/AuNP/SPCE; the electrodes were sealed and kept at 4 °C for a minimum incubation time of 3 h to allow the protein to bind to the AuNPs through thiol-gold bonds. After incubation, the surface of the electrodes was gently rinsed right before each use with PB, pH 7.4, to remove unbound proteins. For each detection step, 30 μL of each sample was placed on the surface of the electrode, and the response of each electrode was recorded by CV.

Surface plasmon resonance measurements

GluBP was immobilized on a CM5 chip (medium density carboxylated dextran surface) in 2.5 mM potassium acetate, pH 6.0, using standard EDC/NHS coupling procedures. Data were fitted to a 1:1 binding model of affinity saturation curves with individual concentrations measured in triplicate. The running buffer was PBS (150 mM NaCl, 2.5 mM KCl, 81 mM Na_2HPO_4, and 14.7 mM KH_2PO_4) supplemented with 1 mM $MgCl_2$. Surface regeneration was achieved with exposure to 3 M $MgCl_2$ for 30 s followed by 5 min reequilibration with running buffer. R_{max} values for different concentrations of glutamate were determined in triplicate. Measurements shown were carried out at flow rates of 20 μL/min without indications of flow-rate dependency when tested at 5-50 μL/min.

Results

Fabrication and characterization of AuNP-modified SPCEs

Three different concentrations (100 μM, 1 mM, and 10 mM) of $HAuCl_4$ were electrochemically deposited on the surface of SPCEs, and SEM was used to evaluate the size, morphology, and density of the generated AuNPs on the surface of the SPCEs. Figure 1, *A* depicts the surface of the SPCEs before deposition of AuNPs. In Figure 1, *B-D*, SEM images show the increased density and size of AuNPs as the concentration of the gold (III) chloride solution increases. The lowest concentration of gold (III) chloride solution (100 μM) generated a lower density of AuNPs with an average size of 20 ± 4 nm (Figure 1, *B*). In comparison, the concentration of 1 mM generated AuNPs with an average size of 56 ± 17 nm (Figure 1, *C*). However, increasing the concentration of the gold (III) chloride solution to 10 mM resulted in a gold aggregate on the surface of the SPCE (Figure 1, *D*). These results indicate that the concentration of the gold solution significantly influences the morphology, size, and quantity of AuNPs deposited on the SPCEs. The presence of the gold nanoparticles on the electrodes that were manufactured with 1 mM starting gold solution was confirmed using EDX (Figure 1, *E*).

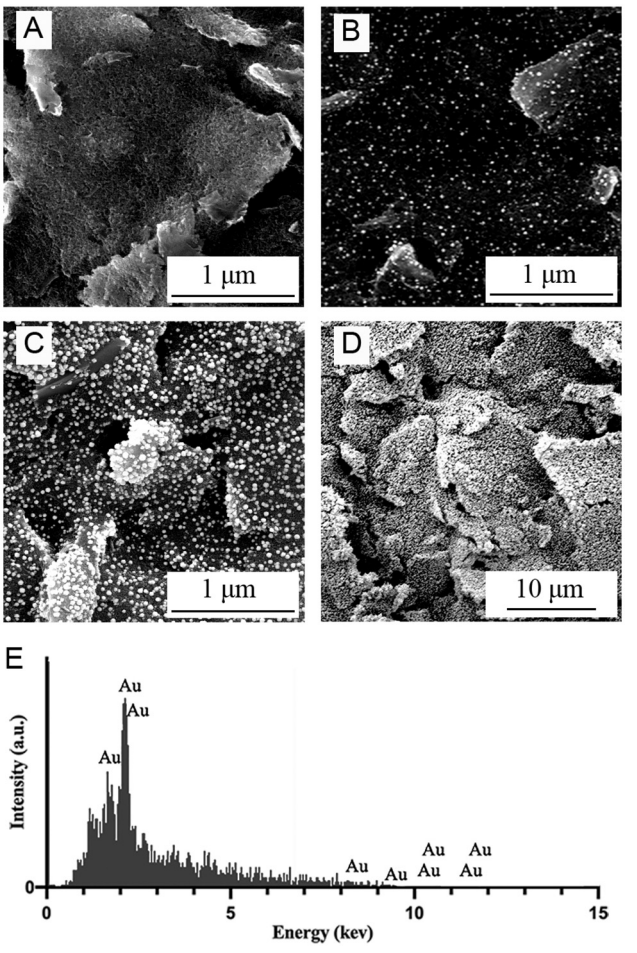

Figure 1. Surface characterization of AuNP-modified SPCEs using scanning electron microscopy: **(A)** bare SPCE. AuNP-modified SPCE through chronoamperometry using **(B)** 100 μM, **(C)** 1 mM, and **(D)** 10 mM gold (III) chloride solution. **(E)** Energy-dispersive X-ray spectrum of the AuNP/SPCE generated using 1 mM gold(III) chloride.

After each step of biosensor fabrication, the response of the electrode was measured by sweeping the potential from −0.2 to 1.0 V in PB, pH 7.4, at a scan rate of 50 mV/s (Figure 2, *A-D*). In the absence of AuNPs on the surface of the electrodes, the SPCEs were redox-inert under these experimental conditions

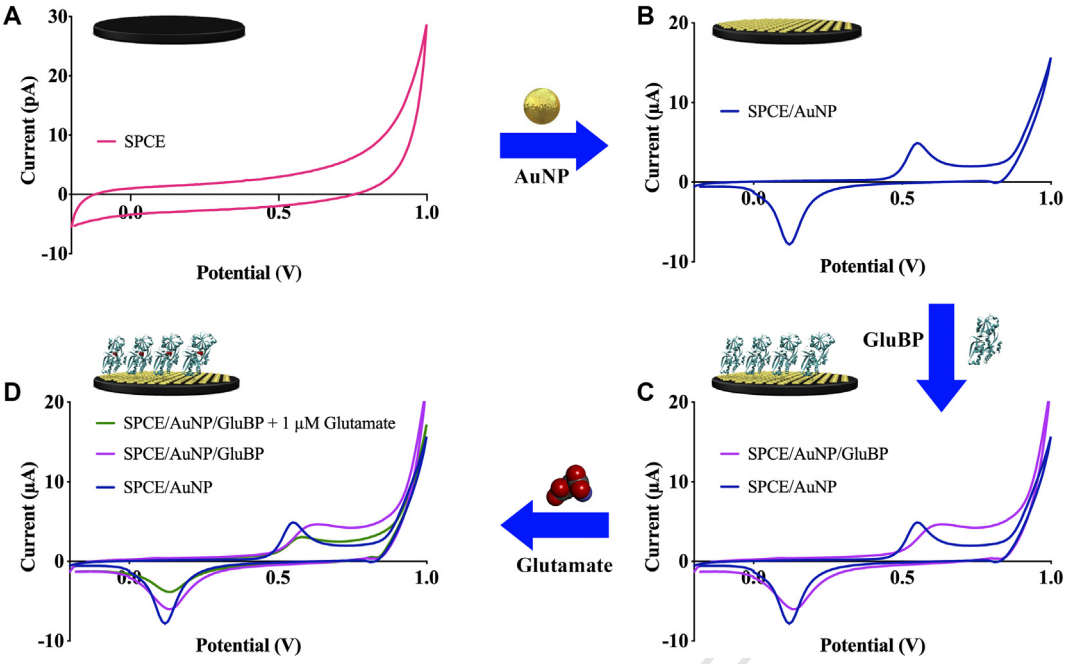

Figure 2. Fabrication and analytical performance of the GluBP-based biosensor. Cyclic voltammograms of **(A)** SPCE, **(B)** AuNP/SPCE, **(C)** GluBP/AuNP/SPCE in PB, and **(D)** GluBP/AuNP/SPCE in the presence of 1 μM glutamate in PB. Scanning range is from −0.2 V to +1.0 V vs. Ag/Ag/Cl at a rate of 50 mV/s in 50 mM phosphate buffer, pH 7.4, for all experimental steps. Inset: Schematics of the surface of the working electrode in the process of the biosensor fabrication.

(Figure 2, *A*). On the other hand, when the electrodes that had been modified with AuNPs were subjected to the same conditions, the generation of gold oxide on the electrode surface was observed at a peak potential of +0.57 V. The formation of the gold oxide layer is reversible, and, during the reverse scan, the gold oxide gets reduced, which was observed as a peak at a potential +0.13 V (Figure 2, *B*). The CV response of the AuNP/SPCEs in the absence of glutamate binding protein was used as the baseline in the subsequent experiments.

Based on the cyclic voltammograms, the peak current intensity of the gold redox reaction is directly related to the size and distribution of the AuNPs on the surface of the electrodes and, therefore, the effective surface area. Increasing the concentration of gold solution during the electrochemical deposition of the AuNPs leads to an increase in the peak current corresponding to the gold redox reaction (Figure S3). The smallest AuNP size that has higher surface area per unit mass generated by electrodeposition using the 100 μM gold (III) chloride solution showed the lowest signal intensity. Another parameter to consider for optimizing the sensor response is the size of the oxidation and reduction peaks of gold; a larger peak will make it difficult to determine the change in current that is occurring due to the protein conformational change (explained in more detail in the analytical performance of the glutamate biosensor) on the surface of the electrode. This high reduction and oxidation peaks could be attributed to the aggregation of gold as observed under SEM, which in turn increases the background noise from the bare gold on the electrodes. Notably, the change in the peak current that happens upon glutamate binding is relatively small in comparison to the bare gold

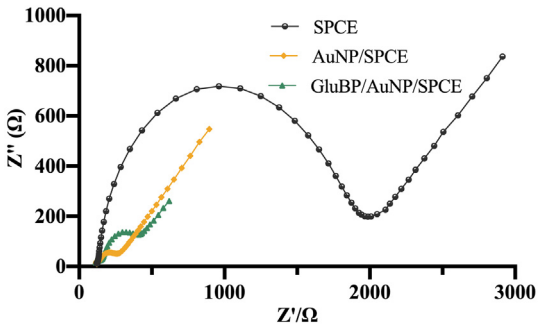

Figure 3. EIS characterization of SPCE, AuNP/SPCE and GluBP/AuNP/SPCE in 10 mM $[Fe(CN)_6]^{3-/4-}$, 50 mM PBS buffer at a potential of +0.18 V vs. Ag/Ag/Cl.

electrode, and thereby the ratio of this change to that of the bare electrodes must be adjusted in a way to minimize the background. This can be achieved by choosing the appropriate AuNP size and density. The size of AuNPs plays an important role on the performance of the biosensor because it determines the extent of protein conjugation to the AuNP.[40] Accordingly, we selected for the remainder of the studies to use electrodes that had nanoparticles deposited by using the 1 mM gold (III) chloride solution; deposition over 5 min under these conditions resulted in AuNP of 56 ± 17 nm.

Glutamate biosensor

The GluBP was genetically engineered to carry two cysteines at the C-terminal to allow the formation of thiol bonds to gold.

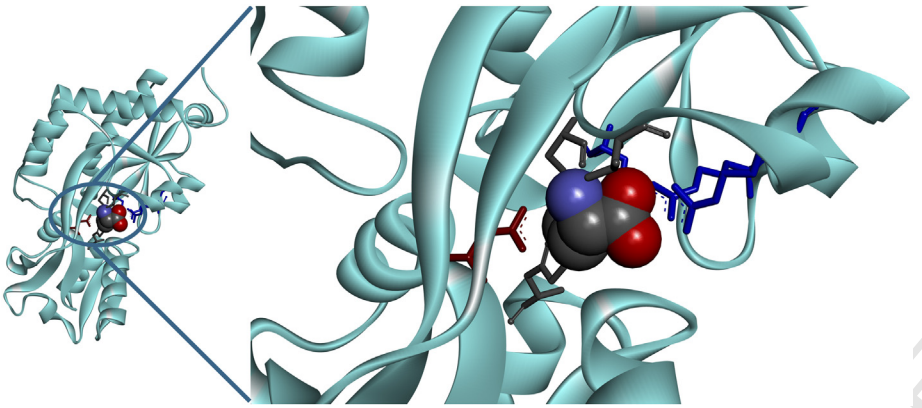

Figure 4. X-ray crystal structure of GluBP[35] demonstrating the binding pocket with charged amino acid residues stabilizing glutamate and neutral amino acid residues forming hydrogen bonds with glutamate: three positively charged arginine residues (blue) interacting with glutamate's α-amino group, negatively charged aspartate residue (red) interacting with glutamate's α-carboxylate group and neutral serine and two threonine residues (gray) forming hydrogen bonds with glutamate. The X-ray crystal structure of the protein was visualized using Studio Visualizer (BIOVIA) by using the coordinates downloaded from RCSB protein data bank (PDBID- 2VHA).

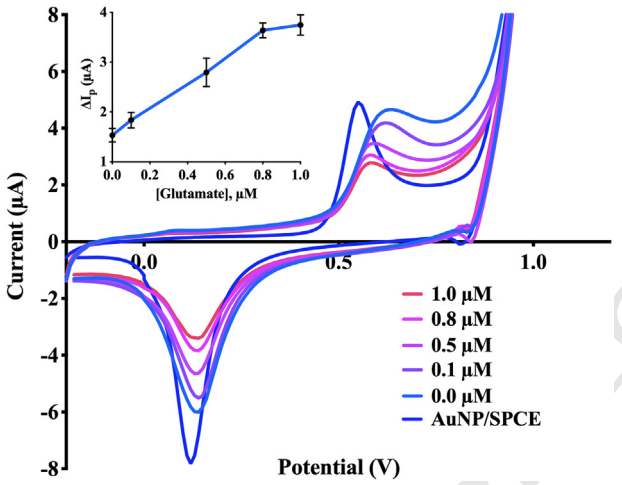

Figure 5. Cyclic voltammograms of AuNP/SPCE in 50 mM PB, pH 7.4, and GluBP/AuNP/SPCE in the presence of different glutamate concentrations (0.0, 0.1, 0.5, 0.8, and 1.0 μM) in the same buffer. Inset: calibration plot for the change in the gold reduction peak current vs glutamate concentration at +0.13 V in triplicate; data are baseline-subtracted using AuNP/SPCE with R^2 value of 0.96 based on the linear portion of the graph.

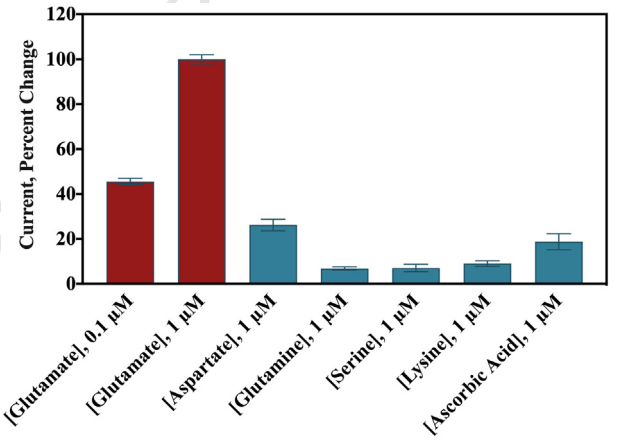

Figure 6. Cross-reactivity of the GluBP-based sensor with other amino acids and ascorbic acid, a common interfering substance. The data represent the percent change of current at +0.13 V in triplicate. Data are baseline-subtracted using AuNP/SPCE.

The presence of the non-conductive protein on the surface of the electrodes reduces the AuNPs active surface area and, therefore, causes the reduction in the peak current observed through CV of GluBP/AuNP/SPCEs (Figure 2, *C*). The CV response of the GluBP/AuNP/SPCE was then measured after addition of 30 μL of 1 μM glutamate in PB, pH 7.4, on the surface of the electrodes under the same conditions and additional decrease in the peak current of gold was observed (Figure 2, *D*).

Electrochemical impedance spectroscopy (EIS)

The protein–gold conjugation was confirmed with electrochemical impedance spectroscopy (EIS). Figure 3 shows the Nyquist plots for the bare SPCE, AuNP/SPCE, and GluBP-based biosensor, which were obtained in 10 mM $[Fe(CN)_6]^{3-/4-}$, 50 mM PBS buffer, pH 7.4, in the frequency range of 100 mHz to 100 MHz at a potential of +0.18 V (vs. Ag/AgCl) with an AC amplitude of 10 mV. A larger semicircle was observed for the SPCE compared to the AuNP/SPCE, which is attributed to the lower conductivity of the bare SPCE versus the AuNP/SPCE. However, after conjugation of the GluBP on the surface of electrode, an increase in the diameter of the semicircle of the Nyquist plot was observed. This is attributed to the electron transfer resistance due to the conjugation of the non-conductive GluBP on the surface of the AuNP/SPCE.

Analytical performance of glutamate biosensor

The ability of GluBP to bind selectively to glutamate can be explained by looking at the charge distribution within the binding pocket of the protein. There are three tightly packed positively charged arginine residues. There are also four

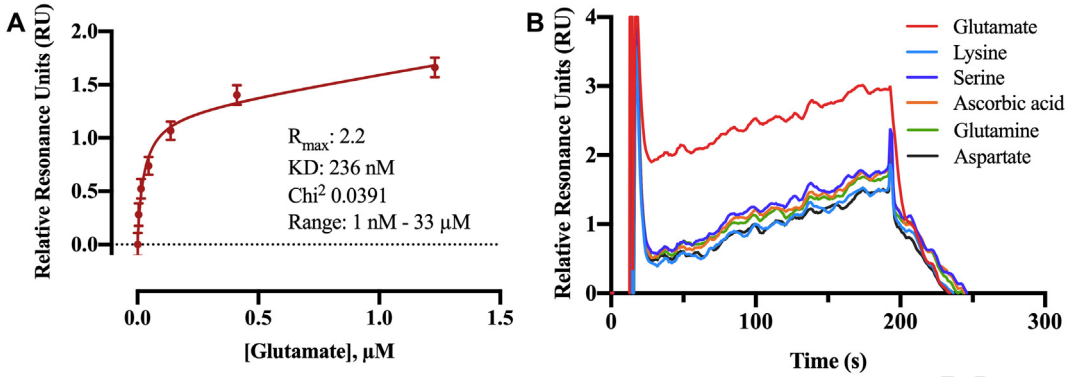

Figure 7. Study of immobilized GluBP with SPR. **(A)** Saturation curve of glutamate binding to immobilized GluBP. The plot shows the R_{max} obtained for the indicated concentrations in triplicate, and data were fit to a 1:1 binding model. Measurements were carried out over a range from 1 nM to 33 µM. A smaller selection is shown for presentation purposes. The indicated K_D and chi^2 reflect the fit over the entire range. **(B)** Immobilized GluBP binds glutamate but does not show significant binding to other potentially interfering compounds when tested at 500 nM. Injection profiles for the different compounds are superimposed for comparison purposes. The graph represents the response after the baseline was subtracted.

negatively charged glutamic acid residues and two negatively charged aspartic acid residues dispersed within the binding cleft of the GluBP (Figure 4). The average charge of the binding pocket is negative, which can prevent most of the negatively charged molecules from binding to GluBP. The charge distribution within the binding pocket is in such a way that the amino group of glutamate is positioned at the negatively charged region, and both carboxylate groups are positioned at the positively charged region.[35] When glutamate binds to GluBP, the conformation of the protein changes. The GluBP binding to glutamate involves a multi-state binding process. The protein exists in equilibrium between partially closed and open conformations.[41] While the protein is immobilized on the surface of the AuNP/SPCEs, the change in protein conformation from the open to the closed state upon binding to glutamate results in alteration of the surface of the electrode which can be measured electrochemically.

The CVs were obtained at bare AuNP/SPCE and GluBP/AuNP/SPCE in the absence and presence of glutamate (Figure 5). Cyclic voltammograms were collected in the potential range of −0.2 to +1.0 V vs. Ag/AgCl in PB, pH 7.4, at a scan rate of 50 mV/s. The peak current responsible for the reduction of the AuNPs, observed at +0.13 V, in GluBP/AuNP/SPCE electrode decreased in the presence of glutamate in the reverse scan. The calibration plot of the difference in the peak current intensities before and after addition of glutamate versus glutamate concentration was plotted, and a linear range of 0.1 µM to 0.8 µM was observed (Figure 5, inset). The detection limit of 0.15 µM was calculated as the concentration that corresponds to three standard deviations above the blank signal,[42] and all the measurements were performed in triplicate with three distinct GluBP/AuNP/SPCEs.

Although the binding pocket of GluBP is very well adapted for binding of glutamate, it is possible that some small molecules could bind and elicit a response from GluBP. Therefore, the response of the fabricated biosensor was measured in the presence of other commonly encountered, small molecules that may interfere with the measurements. Ascorbic acid is a common interfering substance in electrochemical measurements in physiological fluids; lysine is a positively charged amino acid that has the potential to bind to the negatively charged binding pocket of the GluBP, and serine is a small polar/neutral amino acid. Glutamine is a polar amino acid that is structurally similar to glutamate and could potentially interfere with the sensor response. Finally, previous reports demonstrated that GluBP has 10-fold preference to glutamate over aspartate.[43] The concentrations of all possible interfering substances were at 1 µM, and the measurements were performed in triplicate with three separately manufactured GluBP/AuNP/SPCEs (Figure 6). The results demonstrate that the sensor has a preferential response to glutamate, and 1 µM aspartate gave a smaller response than 0.1 µM glutamate. Even smaller responses were obtained with all other potential interferences tested.

The direct binding of glutamate to GluBP was further assessed using surface plasmon resonance (SPR) to confirm the selective binding of GluBP to glutamate. To this end, GluBP was coupled to the surface of a CM5 chip through EDC/NHS coupling.[44] In principle, CM5 chips have a gold surface modified with a carboxy-terminated thiol. The EDC/NHS reaction activates the carboxyl group to facilitate binding of the GluBP on the chips through its native amine residues. Glutamate was allowed to flow over the chip and interact with the immobilized GluBP. Figure 7, *A* shows the result of the effect of different concentrations of glutamate on sensor response (in triplicate). At the selected buffer conditions of PBS with 1 mM magnesium chloride, the curve fit for 1:1 binding, shown in Figure 7, *A*, yields a dissociation constant of 2.4×10^{-7} M. A second chip with immobilized GluBP was evaluated and independently yielded a dissociation constant of 2.1×10^{-7} M under the same buffer conditions (data not shown).

The evaluation of glutamate binding to GluBP by SPR yielded a dissociation constant that is comparable to published data[43] and reproduced in a second independent immobilization of GluBP. During experimental optimization, GluBP demonstrated sensitivity toward harsh surface regeneration procedures of the SPR chip. The best results were obtained with 3 M $MgCl_2$ as the regeneration buffer. The addition of 1 mM $MgCl_2$ in the running buffer provided a more stable baseline and a

reproducible glutamate–GluBP interaction. The specificity of binding was confirmed by comparison to several other compounds (Figure 7, *B*).

For the amount of immobilized GluBP, the maximum relative resonance units (RU) represent approximately 20% of the maximum anticipated signal. While within an acceptable range, this value is relatively low for the binding of a small molecule to its target protein, if steric hindrance were the only limitation to binding. However, binding of glutamate to GluBP involves the opening and subsequent closure of a binding site that is located between the N- and C-terminal domains of GluBP, and therefore requires significant conformational changes and may involve a metastable encounter complex.[41] The observed 20% activity may reflect the nature of the immobilization and interference with the required conformational changes. GluBP couples to a standard CM5 chip with its carboxylated dextran matrix with very high efficiency, potentially linking it to the immobilized surface in ways that restrict movement (or block the binding site of the protein) and thus reduce the number of GluBP molecules capable of binding its ligand.

Discussion

Here we presented the fabrication and characterization of a hybrid electrochemical biosensor for direct glutamate detection. The CV of the fabricated biosensor demonstrated reduction in peak current of AuNP in GluBP/AuNP/SPCE. The change in the peak current was proportional to the concentration of glutamate, which could be explained by the selective binding of glutamate to the GluBP and the corresponding conformational change of the protein. The GluBP binds to glutamate through a multi-state binding process that involves an equilibrium between partially closed (when bound to glutamate) and open structures.[41] Change in the conformation of the protein from the open to the closed state causes a change in the accessible surface of AuNPs on the electrode, which can be detected by CV as a reduction of the current intensities of both oxidation and reduction peaks of gold.

In conclusion, in this study we demonstrate a new platform for analyte detection by incorporating a periplasmic binding protein, GluBP, that undergoes a significant conformational change upon analyte binding. The fabricated enzyme-free, GluBP-based biosensor was effective in measuring glutamate concentrations at physiological pH, with a low limit of detection, and relatively fast response. The sensor had a dose-dependent response for glutamate with a linear response in the range of 0.1 μM to 0.8 μM. The ability of the immobilized GluBP to selectively detect glutamate was explored by both CV and SPR. The described GluBP biosensor system has the potential to be used as a platform for detection of glutamate in biological samples.

Appendix A. Supplementary data

Supplementary data to this article can be found online at https://doi.org/10.1016/j.nano.2020.102305.

References

1. Leibowitz A, Boyko M, Shapira Y, Zlotnik A. Blood glutamate scavenging: insight into neuroprotection. *Int J Mol Sci* 2012;**13**(8):10041-10066.
2. Campos F, Sobrino T, Ramos-Cabrer P, Argibay B, Agulla J, Pérez-Mato M, et al. Neuroprotection by glutamate oxaloacetate transaminase in ischemic stroke: an experimental study. *Journal of Cerebral Blood Flow* 2011;**31**(6):1378-1386.
3. Walton H, Dodd P. Glutamate–glutamine cycling in Alzheimer's disease. *Neurochem Int* 2007;**50**(7–8):1052-1066.
4. Yi J-H, Hazell AS. Excitotoxic mechanisms and the role of astrocytic glutamate transporters in traumatic brain injury. *Neurochem Int* 2006;**48**(5):394-403.
5. Frigo M. G. Cogo M, L. Fusco M, Gardinetti M, Frigeni B. Glutamate and multiple sclerosis. *Curr Med Chem* 2012;**19**(9):1295-1299.
6. Sontheimer H. A role for glutamate in growth and invasion of primary brain tumors. *J Neurochem* 2008;**105**(2):287-295.
7. Li L, Hanahan D. Hijacking the neuronal NMDAR signaling circuit to promote tumor growth and invasion. *Cell* 2013;**153**(1):86-100.
8. Inoshita M, Umehara H, Watanabe S-y, Nakataki M, Kinoshita M, Tomioka Y, et al. *Elevated peripheral blood glutamate levels in major depressive disorder Neuropsychiatric Disease and Treatment* 2018;**14**:945-953.
9. Aliprandi A, Longoni M, Stanzani L, Tremolizzo L, Vaccaro M, Begni B, et al. Increased plasma glutamate in stroke patients might be linked to altered platelet release and uptake. *Journal of Cerebral Blood Flow & Metabolism* 2005;**25**(4):513-519.
10. Koochekpour S, Majumdar S, Azabdaftari G, Attwood K, Scioneaux R, Subramani D, et al. Serum glutamate levels correlate with Gleason score and glutamate blockade decreases proliferation, migration, and invasion and induces apoptosis in prostate cancer cells. *Clin Cancer Res* 2012;**18**(21):5888-5901.
11. Monge-Acuña AA, Fornaguera-Trías J. A high performance liquid chromatography method with electrochemical detection of gamma-aminobutyric acid, glutamate and glutamine in rat brain homogenates. *J Neurosci Methods* 2009;**183**(2):176-181.
12. Tucci S, Pinto C, Goyo J, Rada P, Hernández L. Measurement of glutamine and glutamate by capillary electrophoresis and laser induced fluorescence detection in cerebrospinal fluid of meningitis sick children. *Clin Biochem* 1998;**31**(3):143-150.
13. Yu Y, Sun Q, Zhou T, Zhu M, Jin L, Shi G. On-line microdialysis system with poly(amidoamine)-encapsulated Pt nanoparticles biosensor for glutamate sensing in vivo. *Bioelectrochemistry* 2011;**81**(1):53-57.
14. van den Pol AN. Glutamate and aspartate immunoreactivity in hypothalamic presynaptic axons. *J Neurosci* 1991;**11**(7):2087-2101.
15. Gencoglu A, Minerick AR. Electrochemical detection techniques in micro- and nanofluidic devices. *Microfluidics and Nanofluidics* 2014;**17**(5):781-807.
16. Durairaj S, Sidhureddy B, Cirone J, Chen A. Nanomaterials-based electrochemical sensors for in vitro and in vivo analyses of neurotransmitters. Applied Sciences. 2018;8(9).
17. Tang H, Chen J, Nie L, Kuang Y, Yao S. A label-free electrochemical immunoassay for carcinoembryonic antigen (CEA) based on gold nanoparticles (AuNPs) and nonconductive polymer film. *Biosens Bioelectron* 2007;**22**(6):1061-1067.
18. Ambrosi A, Castañeda MT, Killard AJ, Smyth MR, Alegret S, Merkoçi A. Double-codified gold nanolabels for enhanced immunoanalysis. *Anal Chem* 2007;**79**(14):5232-5240.
19. Jiang P, Wang Y, Zhao L, Ji C, Chen D, Nie L. Applications of gold nanoparticles in non-optical biosensors. Nanomaterials. 2018;8(12).
20. Batra B, Pundir CS. An amperometric glutamate biosensor based on immobilization of glutamate oxidase onto carboxylated multiwalled carbon nanotubes/gold nanoparticles/chitosan composite film modified Au electrode. *Biosens Bioelectron* 2013;**47**:496-501.

AUTHOR QUERY FORM

ELSEVIER	**Journal: NANO** **Article Number: 102305**	**Please e-mail your responses and any corrections to:** **E-mail: Corrections.ESCH@elsevier.spitech.com**

Dear Author,

Please check your proof carefully and mark all corrections at the appropriate place in the proof (e.g., by using on-screen annotation in the PDF file) or compile them in a separate list. Note: if you opt to annotate the file with software other than Adobe Reader then please also highlight the appropriate place in the PDF file. To ensure fast publication of your paper please return your corrections within 48 hours.

For correction or revision of any artwork, please consult http://www.elsevier.com/artworkinstructions.

We were unable to process your file(s) fully electronically and have proceeded by

☐ Scanning (parts of) your article ☐ Rekeying (parts of) your article ☐ Scanning the artwork

Any queries or remarks that have arisen during the processing of your manuscript are listed below and highlighted by flags in the proof. Click on the 'Q' link to go to the location in the proof.

Location in article	Query / Remark: click on the Q link to go Please insert your reply or correction at the corresponding line in the proof
Q1	Your article is registered as a regular item and is being processed for inclusion in a regular issue of the journal. If this is NOT correct and your article belongs to a Special Issue/Collection please contact s.sudhakar@elsevier.com immediately prior to returning your corrections.
Q2	Have we correctly interpreted the following funding source(s) and country names you cited in your article: "National Science Foundation; University of Miami".
Q3	The author names have been tagged as given names and surnames (surnames are highlighted in teal color). Please confirm if they have been identified correctly.
Q4	Supplementary caption was not provided. Please check the suggested data if appropriate, and correct if necessary. Please check this box if you have no corrections to make to the PDF file. ☐

Thank you for your assistance.